Radioactive (^{90}Y) upconversion nanoparticles conjugated with recombinant targeted toxin for synergistic nanotheranostics of cancer

Evgenii L. Guryev[a,1], Natalia O. Volodina[a,1], Natalia Y. Shilyagina[a], Sergey V. Gudkov[a,b,c], Irina V. Balalaeva[a,d], Arthur B. Volovetskiy[a], Alexander V. Lyubeshkin[e], Alexey V. Sen'[f], Sergey A. Ermilov[f], Vladimir A. Vodeneev[a], Rem V. Petrov[g], Andrei V. Zvyagin[a,d,g,h,2], Zhores I. Alferov[i,2], and Sergey M. Deyev[a,g]

[a]The Institute of Biology and Biomedicine, Lobachevsky State University of Nizhny Novgorod, 603950 Nizhny Novgorod, Russia; [b]Department of Experimental Clinical Studies, Moscow Regional Research and Clinical Institute (MONIKI), 129110 Moscow, Russia; [c]Wave Research Center, Prokhorov General Physics Institute of the Russian Academy of Sciences, 119991 Moscow, Russia; [d]Center of Biomedical Engineering, Sechenov University, 119991 Moscow, Russia; [e]Center of Crystallography and Photonics, Russian Academy of Sciences, 119333 Moscow, Russia; [f]Scientific and Technical Center "Amplitude" Ltd., Zelenograd, 124460 Moscow, Russia; [g]M. M. Shemyakin & Yu. A. Ovchinnikov Institute of Bioorganic Chemistry, Russian Academy of Sciences, 117997 Moscow, Russia; [h]Australian Research Council Centre of Excellence for Nanoscale Biophotonics, Macquarie University, Sydney, NSW 2109, Australia; and [i]Nanotechnology Research and Education Centre of Russian Academy of Sciences, St. Petersburg Academic University, 194021 St. Petersburg, Russia

Contributed by Zhores I. Alferov, July 19, 2018 (sent for review June 4, 2018; reviewed by Andrei Kabashin and Joseph Schlessinger)

We report combined therapy using upconversion nanoparticles (UCNP) coupled to two therapeutic agents: beta-emitting radionuclide yttrium-90 (^{90}Y) fractionally substituting yttrium in UCNP, and a fragment of the exotoxin A derived from *Pseudomonas aeruginosa* genetically fused with a targeting designed ankyrin repeat protein (DARPin) specific to HER2 receptors. The resultant hybrid complex UCNP-R-T was tested using human breast adenocarcinoma cells SK-BR-3 overexpressing HER2 receptors and immunodeficient mice, bearing HER2-positive xenograft tumors. The photophysical properties of UCNPs enabled background-free imaging of the UCNP-R-T distribution in cells and animals. Specific binding and uptake of UCNP complexes in SK-BR-3 cells was observed, with separate ^{90}Y- and PE40-induced cytotoxic effects characterized by IC_{50} 140 μg/mL (UCNP-R) and 5.2 μg/mL (UCNP-T), respectively. When both therapeutic agents were combined into UCNP-R-T, the synergetic effect increased markedly, ∼2200-fold, resulting in IC_{50} = 0.0024 μg/mL. The combined therapy with UCNP-R-T was demonstrated in vivo.

theranostics | targeted therapy | combined therapy | nuclear medicine | upconversion nanoparticles

Targeted therapy makes use of high-affinity molecules as carriers of therapeutic agents, such as radioactive isotopes or toxins, to tumor cells (1–4). Targeted therapy drugs are often administered intravenously, eventually homing to target molecules on the surface of tumor cells (5, 6). In this case, radioactive isotope or toxin molecules attached to high-affinity carrier molecules directly affect tumor cells (7). An emerging new-generation approach in biomedicine, called theranostics, relies on the detection of a complex consisting of a carrier molecule and toxic agent. The theranostics concept is realized by employing drugs with dual therapeutics and diagnostics functionality (8–10).

Despite significant side effects, traditional chemo- and radiotherapy remain most widely used therapeutic modalities of cancer therapy owing to their high efficacy (11). The use of two toxic drugs is known to result in a superadditive effect, with a total effect of the drugs (R_{ab}) greater than an arithmetic sum of the constituent toxic effects (R_a, R_b), so that $R_{ab} > R_a + R_b$. The combined radiation therapy and chemotherapy has been reported to achieve an enhanced cancer treatment outcome due to the superadditive effects (12, 13), although the existing protocols suffer from the drug pharmacokinetics inconsistencies and hence are suboptimal. It has been realized that the best outcome is achievable when both toxic agents enter targeted cancer cells at the same time (14, 15).

In this article, we report on realization of this beneficial combined therapeutic approach, which is improved to allow amelioration of side effects. To this aim, we introduce a hybrid biofunctional nanocomplex whose core represents an upconversion nanoparticle (UCNP). Owing to their unique photophysical properties, UCNPs are widely used as a platform for assembling theranostics complexes. Conversion of near-infrared light (NIR) deeply penetrating in biological tissue to the higher photon energy visible, UV and NIR light is among UCNP's most useful properties. The NIR excitation at 980 nm elicits very little autofluorescence in cells and biological tissue, while the excitation light can be efficiently spectrally filtered due to a large spectral shift. UCNP emission is photostable and blinking-free (16, 17).

Two toxic agents—radioactive beta-emitting isotope ^{90}Y used for targeted radionuclide therapy (11), and a highly efficient fragment of exotoxin A from *Pseudomonas aeruginosa* (PE40) (18)—are coupled to the UCNP core and exert toxicity to cancer cells. Beta-emitter ^{90}Y enclosed in the core of UCNP features a short half-life (63 h) and high linear density of the radiation energy transfer, which allows localization of radiation impact

Significance

Emerging cancer nanotechnology enables targeted delivery of substantial payloads of drugs to cancer sites with concomitant reduction of side effects due to the lesser accumulation in the critical organs. This prompts loading of nanocarriers with therapeutic cargo and contrast agents, allowing combined cancer therapy and tumor visualization, respectively. This paper reports the realization of such combined therapy using conjugates of radionuclide yttrium-90–doped upconversion nanoparticles and targeted toxin. The resultant hybrid complex showed high therapeutic efficacy and high imaging contrast both in vitro and in vivo.

Author contributions: E.L.G., N.O.V., S.V.G., I.V.B., S.A.E., V.A.V., R.V.P., A.V.Z., Z.I.A., and S.M.D. designed research; E.L.G., N.O.V., N.Y.S., A.B.V., A.V.L., and A.V.S. performed research; S.A.E. and S.M.D. contributed new reagents or analytic tools; E.L.G., N.O.V., N.Y.S., S.V.G., I.V.B., A.B.V., V.A.V., and A.V.Z. analyzed data; and E.L.G., S.V.G., I.V.B., V.A.V., R.V.P., A.V.Z., Z.I.A., and S.M.D. wrote the paper.

Reviewers: A.K., CNRS; and J.S., Yale University.

The authors declare no conflict of interest.

[1]E.L.G. and N.O.V. contributed equally to this work.

[2]To whom correspondence may be addressed. Email: andrei.zvyagin@mq.edu.au or zhores.alferov@ras.ru.

This article contains supporting information online at www.pnas.org/lookup/suppl/doi:10.1073/pnas.1809258115/-/DCSupplemental.

Published online September 7, 2018.

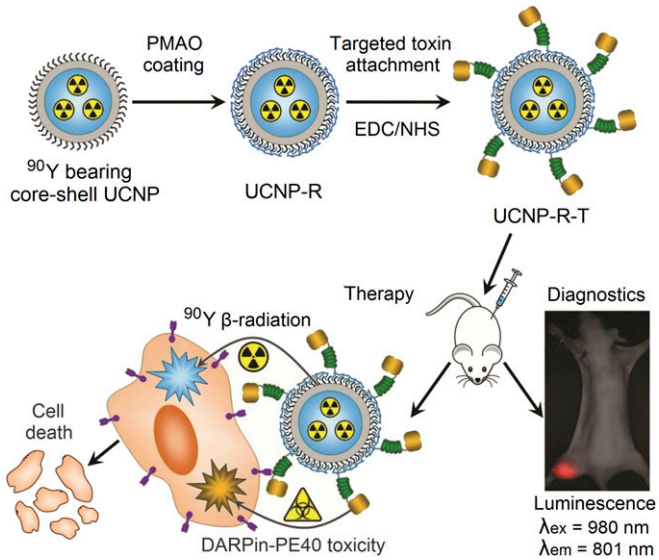

Fig. 1. Assembly and mode of action of the hybrid biofunctional nanocomplex UCNP-R-T. R, radioactive; T, toxic; targeting module, targeted toxin DARPin-PE40. See *Production of a Multifunctional Nanocomplex UCNP-R-T* for details. (Magnification: 2×.)

within several millimeters, leading to reduction of adverse side effects (19, 20). This theranostics complex termed UCNP-R-T contains a targeting biomolecule, which belongs to the class of designed ankyrin repeat proteins (DARPin), and is specific to cells overexpressing HER2 receptors (21, 22). DARPin endows targeting properties to UCNP-R-T. The transmembrane protein HER2 is one of the most well-studied tumor markers; its overexpression represents a hallmark of many types of tumors associated with an increased risk of metastasis and resistance to chemotherapy (23).

This paper reports a superadditive (high-value synergy) toxic effect of the introduced hybrid biofunctional nanocomplex UCNP-R-T on cancer cells. UCNP-R-Ts were demonstrated to inhibit HER2-positive tumor growth in vivo. This synergetic nanocomplex holds promise for applications in tumor diagnostics and therapy.

Results

Production of a Multifunctional Nanocomplex UCNP-R-T. UCNPs of core/shell configuration $NaYF_4$:Yb,Tm/$NaYF_4$ were obtained via two-step synthesis. To render $NaYF_4$ crystal matrix host, doping with ytterbium, Yb^{3+} (20% molar ratio) and thulium, Tm^{3+} (0.6% molar ratio) was done. Yb^{3+} ions function as sensitizers transducing the absorbed excitation energy at 980 nm to Tm^{3+} activator ions. Both excited neighboring Yb^{3+} and Tm^{3+} ions coalesce to transfer Tm^{3+} to the higher excited state via a multistep energy transfer upconversion process from which it emits the higher-energy photoluminescence photons. As a result of the two-step upconversion process, Tm-doped UCNP emits photoluminescence in a spectral band centered at 801 nm (the three-step process results in 474-nm emission) upon the NIR excitation. This photoluminescence falls into the biological tissue transparency window (700–1300 nm) and affords the greater optical imaging depth to conduct whole-body imaging of laboratory animals in vivo (Fig. 1).

Surface-modified UCNP(-R)s were coupled with recombinant protein DARPin-PE40 termed targeted toxin by using well-established (3-dimethylaminopropyl)-*N*′-ethylcarbodiimide hydrochloride/*N*-hydroxysulfosuccinimide sodium salt (EDC/NHS) bioconjugation protocol. DARPin-PE40 represents two recombinant proteins DARPin and PE40 fused together through a hinge-like hydrophilic linker, providing a distance of several nanometers between them, which is sufficient for their independent functioning (24). The targeting module DARPin belongs to the class of designed ankyrin repeat proteins, which represents high-affinity (K_d = 3.8 nM) nonimmunoglobulin scaffolds. The toxic module represents a fragment of exotoxin A from *P. aeruginosa* widely used in biomedical research. Exotoxin A is a highly toxic molecule capable to block the protein synthesis in cells through ADP ribosylation of a translation elongation factor 2 (25).

Protein DARPin-PE40 is capable of specific interaction with HER2 receptor-oncomarker with an affinity characterized by the dissociation constant of K_d = 10.8 nM. Owing to its PE40 fragment, it possesses specific toxicity to HER2-positive tumor cells and can significantly inhibit the growth of HER2-positive tumors (26).

As a result, a hybrid biofunctional nanocomplex (UCNP-R-T) was designed and produced. UCNP-R-T comprised an optically detectable UCNP core coated with amphiphilic polymer maleic anhydride and 1-octadecene (PMAO), with targeted toxin DARPin-PE40 covalently bound to its surface. The UCNP-R-T fragment DARPin-PE40 performed two functions, targeting and therapeutic. Its toxic PE40 module was expected to supplement the therapeutic effect of a beta-emitter ^{90}Y.

Properties of UCNP-R-T. The specific radioactivity of as-synthesized UCNP-R was measured to be 4 MBq/mg. The key optical photoluminescent property of UCNP was characterized by the conversion efficiency (η_{uc}) defined as a ratio of the emitted to absorbed power (27). η_{uc} was measured to be 2% for both UCNP-R and UCNP evaluated at the excitation intensity of 70 W/cm^2 at the wavelength 980 nm. As it is seen in Fig. 2*A*, amphiphilic UCNP-R aqueous colloids were characterized by a mean hydrodynamic diameter of ∼50 nm, and contained a larger-diameter fraction centered at ∼250 nm. As it was estimated by taking into account the particle size distribution, a ratio of the discrete nanoparticles to aggregates was measured to be 25,000 (28). At the same time, as the particle size distribution by number

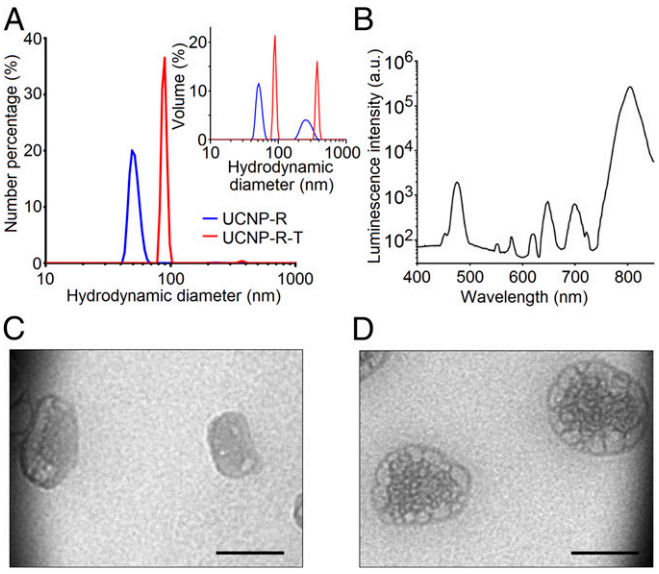

Fig. 2. Characteristics of a hybrid biofunctional nanocomplex UCNP-R-T. (*A*) Particle size distribution by number of upconversion nanoparticles with (UCNP-R-T) and without the targeted toxin (UCNP-R) determined by a dynamic light scattering method. (*Inset*) Particle size distribution by volume, showing the presence of large-size UCNP-R/UCNP-R-T fraction. (*B*) Photoluminescence spectrum of UCNP-R-T upon excitation at the wavelength of 980 nm. (*C*) TEM image of UCNP-R. (Scale bar: 50 nm.) (*D*) TEM image of UCNP-R-T. (Scale bar: 50 nm.)

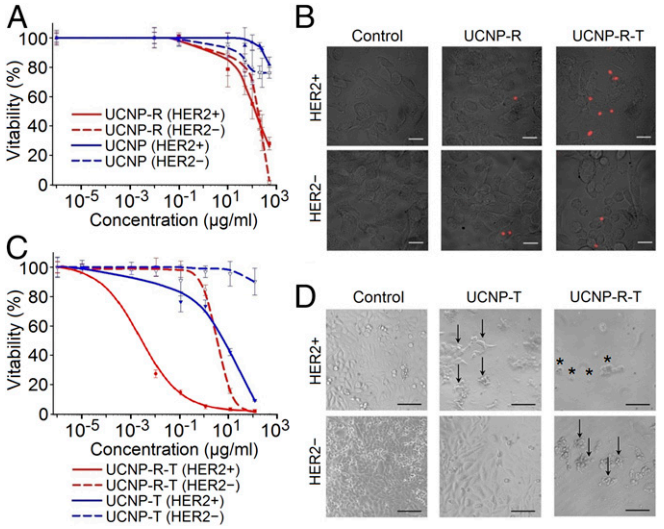

Fig. 3. Interaction of UCNP-R-T with eukaryotic cells. HER2+ denotes SK-BR-3 cells expressing HER2 receptors. HER2− denotes CHO cells lacking HER2 receptors. (*A*) Viability of HER2+ and HER2− cells versus the concentration of UCNP-R and UCNP. (*B*) An overlay of bright-field and fluorescence LSCM images showing specific binding of UCNP-R-T to the surface of HER2+ cells in contrast to little labeling of HER2− cells after 1-h incubation with nanocomplexes at 4 °C. The fluorescence LSCM images were acquired using excitation/emission at 980 nm/769–849 nm. (Scale bars: 20 μm.) (*C*) Viability of HER2+ and HER2− cells versus the concentration of UCNP-R-T and UCNP-T. (*D*) Effects of UCNP-R-T and UCNP-T on the cell morphology. The images were obtained after 96-h incubation with UCNP-R-T/UCNP-T at the concentration of 25 μg/mL. The absorbed dose (in case of UCNP-R-T) was 3.44 Gy per plate well. Arrows indicate detached and shape-changed cells. Asterisks indicate dead cells. (Scale bars: 100 μm.)

indicates (Fig. 2*A*), a major fraction of UCNPs were discrete particles.

The attachment of the targeted toxin to amphiphilic UCNPs increased the mean hydrodynamic diameter to ∼90 and ∼380 nm for discrete particles and aggregates, respectively. The mean diameters of UCNP-Rs and UCNP-RTs calculated based on the transmission electron microscopy data were 35 and 75 nm, respectively (Fig. 2 *C* and *D*) and were smaller than the mean hydrodynamic diameters determined by dynamic light scattering. It was caused by the formation of a Stern layer in aqueous solution.

Fig. 2*B* shows a photoluminescence spectrum of UCNP-R-T upon the excitation at 980 nm. The photoluminescence most pronounced peaks of UCNP-R-T at 475 nm (visible) and 800 nm (NIR) are characteristic for thulium-doped upconversion nanoparticles, confirming their stable suspension in the colloidal samples. The targeted toxin content in UCNP-R-T was evaluated as 2% (51 μg per 1 mg of UCNP-R-T, or ∼50 molecules of targeted toxin per one UCNP-R-T particle), as determined by Bradford method.

Effect of UCNP-R-T on Cancer and Immortalized Cell Cultures. To study the specificity of UCNP-R-T binding to HER2 receptor on the cell surface, a culture of human breast adenocarcinoma cells SK-BR-3 overexpressing HER2 receptors on their surface (HER2+) was used (*SI Appendix*, Fig. S1). Chinese hamster ovary (CHO) cells lacking HER2 receptors were used as a negative control (HER2−). To prevent nanoparticle uptake via the receptor-mediated endocytosis, cells were incubated with UCNP-R-Ts and UCNP-Rs at 4 °C for 1 h. After washing and fixing, the binding of UCNP-R-Ts and UCNP-Rs to the cell surface was detected by fluorescence laser-scanning confocal microscopy (fluorescence LSCM). The acquired images are presented in Fig. 3*B*, where the immobilization of UCNP-R-Ts and UCNP-Rs on the surface membrane of HER2+ SK-BR-3 cells was observable, in contrast with HER2− CHO cells featuring much less nanoparticles.

Toxicity studies of UCNP-R-T and its components were performed using the same SK-BR-3 and CHO cell lines. The concentrations of UCNP-R suspensions used for 96-h incubation corresponded to a range of radiation doses from 20 mGy to 68.8 Gy. Cytotoxicity analysis of nonradioactive UCNP was also carried out to confirm that the cytotoxic effect of UCNP-R was due to ^{90}Y isotope.

UCNP-Rs, in contrast to UCNPs, were found to induce pronounced cytotoxicity (Fig. 3*A*). IC_{50} values for UCNP and UCNP-R lacking the targeted toxin for both cell lines are provided in Table 1. The absorbed dose of the determined concentrations of UCNP-Rs was ∼20 Gy. SK-BR-3 and CHO cells exhibited comparable radiosensitivity.

The concentrations of UCNP-R-T colloids corresponded to the doses absorbed by cells in a range from 1 mGy to 13.6 Gy, while the concentration of DARPin-PE40 corresponded to a range from 83 to 8.3×10^6 pM. Cytotoxicity analysis of nonradioactive nanocomplexes UCNP-T carrying targeted toxins confirmed a synergistic increase in the cytotoxicity of UCNP-R-T due to the combined action of the targeted toxin DARPin-PE40 and radioactive isotope ^{90}Y (Fig. 3*C*). The IC_{50} values of UCNP-R-T and UCNP-T complexes are provided in Table 1. The coupling of targeted toxin DARPin-PE40 to UCNP-R resulted in a 39- and ∼10^5-fold increase of the toxic effect against HER2− and HER2+ cells, respectively, indicating a high specificity of the combined toxic effect to UCNP-R-T.

Thus, the toxicity of UCNP-R-T containing both beta emitters and targeted toxins was significantly greater than the summed-up toxicities of nanoparticles containing only beta emitters (UCNP-R) or only targeted toxins (UCNP-T). UCNP-R-Ts diminished the viability of HER2+ cells substantially (IC_{50} = 0.0024 μg/mL in comparison with 4.2 μg/mL for HER2− cells) (Table 1). Bright-field imaging of the tested cells revealed profound morphological changes of HER2− cells, including detachment of cells from the substrate and alterations in linear dimensions, while HER2+ cells exhibited pronounced death of the entire monolayer (Fig. 3*D*).

To assess the type of interaction of the UCNP-R-T components, the combination index (*CI*) was calculated, using the toxicity data of the UCNP-R-T components in the cases of the separate and combined (as part of UCNP-R-T) administration. The calculated *CI* value of 4.8×10^{-4} was in the region of low values (*CI* << 1), indicating a strong synergism of the toxic modules within UCNP-R-T. It can be inferred that the combination of two agents in one hybrid biofunctional nanocomplex allowed it to synergistically increase its therapeutic efficacy (superadditive effect) in cell culture model; in particular, the targeted toxin DARPin-PE40 endowed UCNP-R-T remarkable specific cytotoxicity to target HER2+ cells.

Therapeutic Effects of UCNP-R-T. Anticancer efficacy of UCNP-R-T was investigated on immunodeficient BALB/c nude mice, bearing HER2-positive human xenograft tumors. Tested colloidal UCNP-based nanocomplexes were administered intratumorally at doses of 10 and 15 μg/g. This administration route was chosen

Table 1. Effect of nanocomplexes of various composition on the survival of HER2+ SK-BR-3 cells and HER2− CHO cells

	IC_{50},* μg/mL			
Cell type	UCNP	UCNP-R	UCNP-T	UCNP-R-T
HER2+	>>1,000	140 (94–209)	5.2 (3.2–9.5)	0.0024 (0.0009–0.0058)
HER2−	>>1,000	162 (118–223)	>100	4.2 (1–17.8)

*IC_{50} values are given with 95% confidence interval.

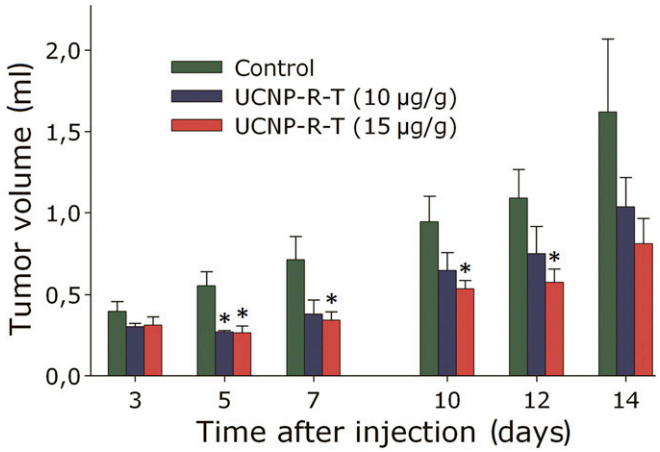

Fig. 4. Therapeutic effect of UCNP-R-T. Dynamics of the tumor volume in mice upon treatment with UCNP-R-T at doses of 10 and 15 μg/g. The tumor node volume is normalized to that measured on day 0 (day of UCNP-R-T administration). The data are presented as mean ± SEM. * denotes statistically significant difference from the control ($P < 0.05$), according to t test with Bonferroni correction, $n = 5–10$.

to reduce systemic toxic effect on the animal organism, enhance the local therapeutic effect, and increase retention time of the tested hybrid biofunctional nanocomplexes in the tumor. We note that although intravascular injection represents the more realistic modeling of UCNP-R-T clinical applications of systemic oncotherapy, the key challenge of UCNP-R-T deposition in critical organs (liver, spleen, etc.) must be addressed.

It was demonstrated that the application of UCNP-R-T at doses of 10 and 15 μg/g resulted in a statistically significant reduction of the volume of the tumor node, compared with that of the control group (Fig. 4). UCNP-R-T was shown to exert the highest anticancer effect at a dose of 15 μg/g, where the tumor growth rate decreased most prominently, as measured by a tumor growth inhibition (*TGI*) factor presented in *SI Appendix*, Fig. S2*A*. The *TGI* of >40% was achieved with a single intratumoral administration of UCNP-R-T at a dose of 15 μg/g throughout the experiment, with >50% inhibition at days 5 and 7. The tumor growth was inhibited by 40% up to day 7, following UCNP-R-T administration at a dose of 10 μg/g, with subsequent inhibition not exceeding 30%. (Please see *SI Appendix* for additional data and analysis of the anticancer efficacy of UCNP-R-T in vivo.)

We quantified half time of UCNP-R-T retention in tumor and the radiation load on tumor cells by performing analysis of the tumor growth data and UCNP distribution in the tumors using a home-built whole-animal imaging system, with the main results presented in Fig. 5*A*. Since the intensity of UCNP photoluminescence is independent of the radioactive ^{90}Y presence, its time evolution reflected the pharmacokinetics of UCNP-R-T in the tumor node. Based on the analysis of the photoluminescence imaging data, the half-life of UCNP-R-T in the tumor node was calculated as 150 h (~6 d) (Fig. 5*B*).

To determine the apparent level of UCNP-R-T radioactivity in the tumor versus time, both radioactive decay of ^{90}Y and UCNP-R-T clearance from the tumor had to be taken into account. The time of twofold decrease of the ^{90}Y content in the tumor Δt was determined by the following equation:

$$1/\Delta t = 1/T + 1/\tau, \qquad [1]$$

where T is the half-life of ^{90}Y and τ is the half time of the nanocomplex clearance from the tumor. ^{90}Y isotope half-life is known to be 64 h. Δt was calculated to be 45 h (~2 d) (Fig. 5*B*). The results were corrected on 30% clearance from the tumor of the administrated UCNP-R-T within the first 3 h postinjection.

The specific radioactivity in the tumor following an intratumoral administration of UCNP-R-T with initial radioactivity of 0.8 MBq (10 μg/g) and 1.2 MBq (15 μg/g) was calculated using the radioactivity decrease in the tumor node (Fig. 5*C*) and its volume versus time. The therapeutic load was determined as a number of decay events that occurred in the tumor over the exposure time $\Delta N(t')$ given the fixed average energy of decay of 1 MBq. It was calculated by performing integration of the experimentally measured radioactivity of UCNP-R-T nanodrug in the tumor over time:

$$\Delta N(t') = \int_0^{t'} A_0 e^{-\ln 2(t/\Delta t)} dt = A_0 \frac{\Delta t}{\ln 2}\left(1 - e^{-\ln 2(t'/\Delta t)}\right), \qquad [2]$$

where A_0 is the initial radioactivity of UCNP-R-T and Δt is the time of a twofold decrease of UCNP-R-T content in the tumor.

The radiation dose in the tumor was calculated as the energy release upon radioactive decay of ^{90}Y isotopes divided by the volume of a tumor node. Since rapid proliferation of cancer cells was a major contributor to the observed high growth rate of a tumor node, the radiation dose rate represented the most useful parameter for evaluating the therapeutic efficacy of UCNP-R-T. It was found that the radiation dose rate fell to 200 kBq/g at day 5 following an administration of 10 μg/g UCNP-R-T which is below therapeutically significant values (29), and completely diminished by day 10. Administration of 15 μg/g UCNP-R-T

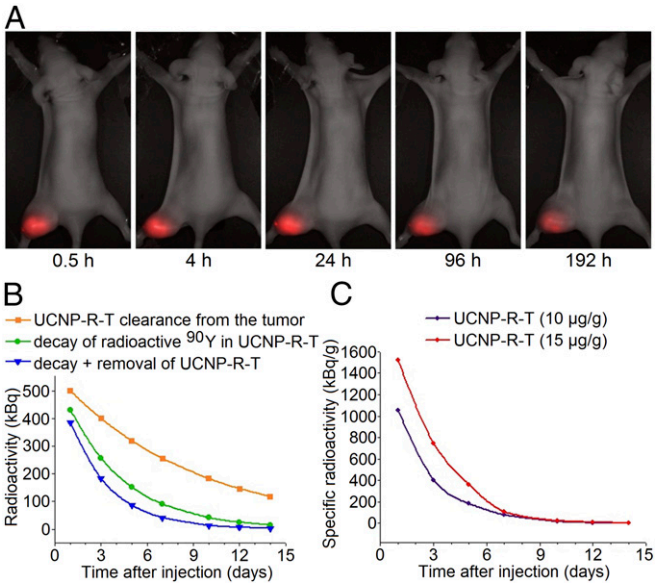

Fig. 5. Retention and activity of UCNP-R-T in the human breast adenocarcinoma SK-BR-3 xenografts on athymic mice. (*A*) Retention of UCNP-R-Ts in the tumor. A time-lapse series of the overlays of the bright-field and epiluminescence images of a tumor-bearing mouse acquired by a home-built whole-animal imaging system. The excitation/emission in the epiluminescence mode, 980 nm/485–831 nm. The images were captured at specified time intervals, following an intratumoral injection of UCNP-R-T at a dose of 10 μg/g. (Magnification: 2×.) (*B*) Dynamics of the radioactivity decrease in the tumor following an intratumoral injection of UCNP-R-T at a dose of 10 μg/g. The initial radioactivity was 0.8 MBq. Upper (orange rectangles), middle (green circles), and lower (blue triangles) curves show decrease of the UCNP-R-T radioactivity in the tumor due to ^{90}Y decay, UCNP-R-T clearance from the tumor calculated based on UCNP photoluminescence, and combined effects of ^{90}Y decay plus UCNP-R-T clearance. (*C*) Time evolution of the specific radioactivity of UCNP-R-T following an intratumoral injection at doses of 10 μg/g (0.8 MBq) and 15 μg/g (1.2 MBq).

resulted in the ~1.2-fold slower decrease of the radiation rate, implying the longer anticancer therapeutic effect.

Taken together, in vivo study of UCNP-R-T effect on human breast HER2+ adenocarcinoma xenografts revealed a statistically significant anticancer effect upon an intratumoral administration at a dose of ~15 μg/g.

Discussion

Currently, there is a trend toward increasing efficiency of anticancer therapy by development of new approaches of personalized medicine, which rely on diagnostics of the molecular profiles of malignant tumors. This allows significant improvement of the treatment outcomes by using drugs with selective effect on target cancer cells. However, most of the drugs developed and deployed for targeted therapy, including those based on inorganic nanoparticles, exhibit relatively low targeting efficiency and significant systemic toxicity, hampering the achievement of optimal therapeutic outcomes (30, 31). One of the approaches to ameliorate these problems is based on enhancement of the targeting performance of new-generation drugs (32–34). A hybrid biofunctional anticancer nanocomplex (upconversion nanoparticle core with embedded beta-emitter ^{90}Y coated with amphiphilic polymer and coupled to targeted toxin DARPin-PE40 termed UCNP-R-T) designed, produced ,and tested in this work is classified as a targeted theranostic agent, which enables both diagnostics and treatment of malignant neoplasms. More specifically, the developed nanodrug addresses oncotherapy of HER2 positive cancers.

The ability of UCNP-R-T to selectively bind to target cells along with its unique photoluminescent properties determines its diagnostic utility (Fig. 5*A*). The UCNP-originated photoluminescence in the visible and NIR spectral regions enables up to 1-cm imaging depth, making it possible to monitor pharmacokinetics of UCNP-R-T in animal model xenografts and potentially in millimeter-sized tumor foci. A vast majority of reports, including our own studies, supports a notion that UCNP complexes exert no cytotoxic effects and no toxic effects on the organs of laboratory animals, or seldom, weak toxic effects (35–38). The existing body of evidence suggests that UCNP-PMAO-s are safe to use as a universal platform for theranostics applications.

Therapeutic potential of the developed hybrid biofunctional anticancer nanocomplex UCNP-R-T is determined by its two effective components: a recombinant targeted toxin DARPin-PE40 and beta-emitter ^{90}Y. High cytotoxicity of the targeted toxin DARPin-PE40 against HER2-positive cells and the relative resistance of HER2-negative cells to its action have been previously established (22). Radionuclide ^{90}Y is a well-known potent therapeutic agent. The proposed technology of UCNP-R-T synthesis allows it to modulate the activity of the nanocomplex over a wide range by changing a proportion of a stable high-abundance yttrium isotope in the composition of UCNP via partial substitution by a radioactive isotope ^{90}Y. This provides a possibility to modulate the cytotoxic effect of UCNP-R-T mediated by beta radiation to achieve optimal therapeutic outcome with minimal side effects on normal organs and tissues. Unlike radioactively stable UCNP, UNCP-R exerts a pronounced cytotoxic effect in cell cultures in the concentration range of 10^{-6}–10^{3} μg/mL (Fig. 3). It is worth mentioning that ^{90}Y is embedded in the core of UCNP, thus its decay products of unknown biological hazard are retained in the nanocrystalline matrix ensured by the strong crystalline bonds. This mitigates toxicological stress stemming from decay products on tissues around the tumor and diminishes adverse side effects.

The existing targeted therapy drugs often contain one toxic module, which can be either a toxin or radioactive isotope, while drugs with two toxic modules are much rarer (39, 40), and just emerging to furnish the concept of combined oncotherapy. Application of drugs with two toxic modules is of particular interest, since both toxic agents enter cancer cells at the same time. Their pharmacokinetics is mutually consistent and in some cases they can demonstrate strong synergism in the combined toxic effect (14). The developed UCNP-R-T carries two toxic modules—beta emitter ^{90}Y and targeted toxin DARPin-PE40, which exert toxic effects on tumor cells by different mechanisms. We found that UCNP-R-T had a significantly greater toxic effect in comparison with just radioactive UCNP (UCNP-R) that provided an equal dose of ionizing radiation. A strong synergism in the toxic effect ($CI << 1$) was observed upon the use of two toxic modules, i.e., the total effect of the two toxicants was more than an order of magnitude greater than a sum of the separate toxic effects.

We speculate the targeted toxin blocks protein synthesis in the cells, which eventually results in their apoptosis (22), while a beta-emitter ^{90}Y causes the formation of free radicals and reactive oxygen species in the cells, along with direct damage of macromolecules (41). A significant increase in the toxicity of UCNP-R-T compared with its individual modules was due to damage of the protein synthesis involved in the antioxidant protection and repair of the ionizing radiation-mediated damage. The precise mechanism behind the observed strong synergy warrants further studies.

Tumors are typically characterized by cellular heterogeneity (42, 43). Oncotherapy based on administration of monodrugs suffers from poor therapeutic efficacy, in addition to the development of multiple drug resistance (44). UCNP-R-T nanocomplex featuring two toxic modules of differing therapeutic actions is believed to be more potent in the treatment of heterogeneous tumors with reduced drug resistance.

UCNP-R-T inhibited the growth of xenograft tumors upon an intratumoral administration. Apparently, this effect was due to the local action of both therapeutic agents and their long-term retention in the tumor enhanced by the targeting protein DARPin module, and because of a larger dose of the ionizing radiation absorbed by the tumor tissue. The absorbed dose of the ionizing radiation (per unit of tumor volume with regard to its growth) reached a maximum value on day 5 after the UCNP-R-T administration, which agreed with the highest rate of the *TGI* observed at the same time point. The obtained results show promise for effective combined oncotherapy leading to prospective translation to clinical practices.

Methods

Synthesis of UCNP-R and UCNP. UCNP-R and UCNPs core/shell nanostructures of the composition $NaY_{0.78}Yb_{0.2}Tm_{0.02}F_4/NaYF_4$ were synthesized as described earlier (45), with modifications. A solution of $^{90}YCl_3$ (SSC RF-IPPE) with a specific activity of 290 MBq/mg was neutralized to pH 9.0, and the precipitate [$^{89}Y(OH)_3/^{90}Y(OH)_3$] was washed with deionized water. Hydrogen peroxide solution was added to the precipitate and the mixture was incubated for 2 h at 700 °C until $^{90}Y_2O_3$ was formed. A mixture of $^{89}Y_2O_3/^{90}Y_2O_3$ (0.78 mM) (or $^{89}Y_2O_3$ for UCNP), Yb_2O_3 (0.2 mM), and Tm_2O_3 (0.02 mM) (Sigma-Aldrich) was alloyed, purified, and coated. The obtained core/shell UCNP-Rs and UCNPs were precipitated.

Producing of DARPin-PE40 Protein and Assembly of UCNP-R-T. Recombinant targeted toxin DARPin-PE40 was prepared as described previously (22). This protein was expressed in *Escherichia coli* BL21 (DE3) cells transformed with plasmid pDARP-PE40 and purified by metal chelate affinity and ion-exchange chromatography. The surface of UCNP-R/UCNP was functionalized by coating with alternating copolymer of PMAO (Sigma-Aldrich) (46). DARPin-PE40 was covalently attached to UCNP-R/UCNP using EDC and Sulfo-NHS linking agents (see *SI Appendix* for details).

Characterization of UCNP-R-T. Concentration of UCNP-R-T was estimated from the radioactivity measurement. Mean hydrodynamic diameter and zeta potential of UCNP-R-T/UCNP-R particles were determined using Zetasizer Nano ZS system. Photoluminescence spectra of UCNP-R-T upon excitation at 980 nm were acquired using CM2203 spectrofluorometer (SOLAR). Study of the other properties of UCNP-R-T is described in *SI Appendix*.

Specificity of UCNP-R-T Binding to the Cell Surface and in Vitro Cytotoxicity Assay. The specificity of UCNP-R-T binding to the cell surface and the cytotoxicity of the UCNP-R-T/UCNP-T/UCNP-R/UCNP were studied on human breast adenocarcinoma (SK-BR-3) and CHO cell lines (see *SI Appendix* for details).

The *CI* of the UCNP-R-T components was calculated by a median-effect method (47):

$$CI = D_1/DX_1 + D_2/DX_2, \quad [3]$$

where DX_1 and DX_2 are IC_{50} of individual toxic modules of UCNP-R-T; D_1 and D_2 are IC_{50} of toxic modules upon coadministration, as a part of UCNP-R-T.

The changes in the cell morphology after incubation with UCNP-R-T/UCNP-T were studied by transmitted light microscopy, using an Axiovert 200 microscope (Carl Zeiss).

Animal Study. All experimental procedures were approved by the Bioethics Committee of Nizhny Novgorod State University. Experiments were conducted in strict accordance with Act 708n (23.08.2010) with the National Ministry of Public Health of Russian Federation approving the rules of laboratory practice for the care and use of laboratory animals and Council Directive 2010/63EU of the European Parliament (22 September 2010) on the protection of animals used for scientific purposes.

The therapeutic effects of UCNP-R-T were studied on BALB/c nude athymic mice bearing SK-BR-3 xenografts (tumor grafting and injection doses are described in *SI Appendix*). After UCNP-R-T injection, the volume of tumors and animal weight were measured every 48 h. The tumor node volume (V) was calculated as $V = \text{length} \times \text{width}^2/2$ (48). *TGI* was calculated using the equation

$$TGI = (V_{control} - V_{treatment})/V_{control} \times 100\%, \quad [4]$$

where V is the average volume of the tumor node in the corresponding group.

The time of the UCNP-R-T retention in the tumor was determined by means of the imaging of experimental tumors using a home-built whole-animal system (49), which allowed detection of photoluminescent signal at a wavelength of 800 nm upon the excitation at 980 nm. Images were taken using an electron multiplying charge-coupled devices (EMCCD) camera with a 2× magnification. Image analysis was performed using ImageJ 1.47v software. The signal in the tumor was determined as a difference between the average fluorescence intensity in the tumor area and the mean photoluminescent intensity of normal tissues.

ACKNOWLEDGMENTS. This work was supported by the Ministry of Education and Science of the Russian Federation (Project 14.Z50.31.0022).

1. Curcio CG, et al. (1976) Short-term results of combined radioimmunotherapy in inoperable lung cancer. *Tumori* 62:587–598.
2. Rosenberg SA, Terry WD (1977) Passive immunotherapy of cancer in animals and man. *Adv Cancer Res* 25:323–388.
3. Perl AE (2017) The role of targeted therapy in the management of patients with AML. *Blood Adv* 1:2281–2294.
4. Mitchell MJ, Jain RK, Langer R (2017) Engineering and physical sciences in oncology: Challenges and opportunities. *Nat Rev Cancer* 17:659–675.
5. Gong W, et al. (2017) Toward the use of precision medicine for the treatment of head and neck squamous cell carcinoma. *Oncotarget* 8:2141–2152.
6. Kobayashi H, Turkbey B, Watanabe R, Choyke PL (2014) Cancer drug delivery: Considerations in the rational design of nanosized bioconjugates. *Bioconjug Chem* 25:2093–2100.
7. Maffioli L, et al. (2015) New radiopharmaceutical agents for the treatment of castration-resistant prostate cancer. *Q J Nucl Med Mol Imaging* 59:420–438.
8. Josefsen LB, Boyle RW (2012) Unique diagnostic and therapeutic roles of porphyrins and phthalocyanines in photodynamic therapy, imaging and theranostics. *Theranostics* 2:916–966.
9. Ma Y, Mou Q, Wang D, Zhu X, Yan D (2016) Dendritic polymers for theranostics. *Theranostics* 6:930–947.
10. Satterlee AB, Huang L (2016) Current and future theranostic applications of the lipid-calcium-phosphate nanoparticle platform. *Theranostics* 6:918–929.
11. Gudkov SV, Shilyagina NY, Vodeneev VA, Zvyagin AV (2016) Targeted radionuclide therapy of human tumors. *Int J Mol Sci* 17:E33.
12. Steel GG, Peckham MJ (1979) Exploitable mechanisms in combined radiotherapy-chemotherapy: The concept of additivity. *Int J Radiat Oncol Biol Phys* 5:85–91.
13. Seiwert TY, Salama JK, Vokes EE (2007) The concurrent chemoradiation paradigm–General principles. *Nat Clin Pract Oncol* 4:86–100.
14. Tian L, et al. (2017) Radionuclide I-131 labeled albumin-paclitaxel nanoparticles for synergistic combined chemo-radioisotope therapy of cancer. *Theranostics* 7:614–623.
15. Yi X, et al. (2015) Imaging-guided combined photothermal and radiotherapy to treat subcutaneous and metastatic tumors using iodine-131-doped copper sulfide nanoparticles. *Adv Funct Mater* 25:4689–4699.
16. Sreenivasan VK, Zvyagin AV, Goldys EM (2013) Luminescent nanoparticles and their applications in the life sciences. *J Phys Condens Matter* 25:194101.
17. Grebenik EA, Kostyuk AB, Deyev SM (2016) Upconversion nanoparticles and their hybrid assemblies for biomedical applications. *Russ Chem Rev* 85:1277–1296.
18. Sokolova E, et al. (2017) HER2-specific recombinant immunotoxin 4D5scFv-PE40 passes through retrograde trafficking route and forces cells to enter apoptosis. *Oncotarget* 8:22048–22058.
19. Audi G, Wapstra AH, Thibault C, Blachot J, Bersillon O (2003) The NUBASE evaluation of nuclear and decay properties. *Nucl Phys A* 729:3–128.
20. Lyra ME, et al. (2013) Radionuclides used in nuclear medicine therapy–From production to dosimetry. *Curr Med Imaging Rev* 9:51–75.
21. Steiner D, Forrer P, Plückthun A (2008) Efficient selection of DARPins with sub-nanomolar affinities using SRP phage display. *J Mol Biol* 382:1211–1227.
22. Sokolova E, et al. (2016) Recombinant targeted toxin based on HER2-specific DARPin possesses a strong selective cytotoxic effect in vitro and a potent antitumor activity in vivo. *J Control Release* 233:48–56.
23. Deyev SM, et al. (2015) Man-made antibodies and immunoconjugates with desired properties: Function optimization using structural engineering. *Russ Chem Rev* 84:1–26.
24. Proshkina GM, Shilova ON, Ryabova AV, Stremovskiy OA, Deyev SM (2015) A new anticancer toxin based on HER2/neu-specific DARPin and photoactive flavoprotein miniSOG. *Biochimie* 118:116–122.
25. Weldon JE, et al. (2013) A recombinant immunotoxin against the tumor-associated antigen mesothelin reengineered for high activity, low off-target toxicity, and reduced antigenicity. *Mol Cancer Ther* 12:48–57.
26. Deyev SM, Lebedenko EN (2017) [Targeted bifunctional proteins and hybrid nanoconstructs for cancer diagnostics and therapies]. *Mol Biol (Mosk)* 51:907–926. Russian.
27. Grebenik EA, et al. (2013) Feasibility study of the optical imaging of a breast cancer lesion labeled with upconversion nanoparticle biocomplexes. *J Biomed Opt* 18:76004.
28. Bobylev AG, Pen'kov NV, Troshin PA, Gudkov SV (2015) [Effect of dilution on aggregation of nanoparticles of polycarboxylic derivative of fullerene C60]. *Biofizika* 60:38–43. Russian.
29. Zhang M, et al. (2009) Preclinical evaluation of an anti-CD25 monoclonal antibody, 7G7/B6, armed with the beta-emitter, yttrium-90, as a radioimmunotherapeutic agent for treating lymphoma. *Cancer Biother Radiopharm* 24:303–309.
30. Choi HS (2014) Nanoparticle assembly: Building blocks for tumour delivery. *Nat Nanotechnol* 9:93–94.
31. Feng Q, et al. (2017) Self-assembly of gold nanoparticles shows microenvironment-mediated dynamic switching and enhanced brain tumor targeting. *Theranostics* 7:1875–1889.
32. Ruan S, et al. (2015) Tumor microenvironment sensitive doxorubicin delivery and release to glioma using angiopep-2 decorated gold nanoparticles. *Biomaterials* 37:425–435.
33. Chou LY, Zagorovsky K, Chan WC (2014) DNA assembly of nanoparticle superstructures for controlled biological delivery and elimination. *Nat Nanotechnol* 9:148–155.
34. Melemenidis S, et al. (2015) Molecular magnetic resonance imaging of angiogenesis in vivo using polyvalent cyclic RGD-iron oxide microparticle conjugates. *Theranostics* 5:515–529.
35. Xiong L, Yang T, Yang Y, Xu C, Li F (2010) Long-term in vivo biodistribution imaging and toxicity of polyacrylic acid-coated upconversion nanophosphors. *Biomaterials* 31:7078–7085.
36. Yu XF, et al. (2010) Neurotoxin-conjugated upconversion nanoprobes for direct visualization of tumors under near-infrared irradiation. *Biomaterials* 31:8724–8731.
37. Abdul Jalil R, Zhang Y (2008) Biocompatibility of silica coated NaYF(4) upconversion fluorescent nanocrystals. *Biomaterials* 29:4122–4128.
38. Kumar R, Nyk M, Ohulchanskyy TY, Flask CA, Prasad PN (2009) Combined optical and MR bioimaging using rare Earth ion doped NaYF4 nanocrystals. *Adv Funct Mater* 19:853–859.
39. Masoud V, Pagès G (2017) Targeted therapies in breast cancer: New challenges to fight against resistance. *World J Clin Oncol* 8:120–134.
40. Zou L, et al. (2016) Current approaches of photothermal therapy in treating cancer metastasis with nanotherapeutics. *Theranostics* 6:762–772.
41. Ward JF (1988) DNA damage produced by ionizing radiation in mammalian cells: Identities, mechanisms of formation, and reparability. *Prog Nucleic Acid Res Mol Biol* 35:95–125.
42. Pitot HC, Cardelli J (1977) Contribution of the Morris hepatomas to the biochemistry of cancer–Establishment of the phenotypic heterogeneity of neoplasms in vivo. *Adv Exp Med Biol* 92:21–37.
43. Fidler IJ (1978) Tumor heterogeneity and the biology of cancer invasion and metastasis. *Cancer Res* 38:2651–2660.
44. Arias JL (2011) Drug targeting strategies in cancer treatment: An overview. *Mini Rev Med Chem* 11:1–17.
45. Mai H, Zhang Y, Sun L, Yan C (2007) Highly efficient multicolor up-conversion emissions and their mechanisms of monodisperse NaYF4:Yb,Er core and core/shell-structured nanocrystals. *J Phys Chem C* 111:13721–13729.
46. Grebenik EA, et al. (2014) Specific visualization of tumour cells using upconversion nanophosphors. *Acta Naturae* 6:48–53.
47. Chou TC, Talalay P (1981) Generalized equations for the analysis of inhibitions of Michaelis-Menten and higher-order kinetic systems with two or more mutually exclusive and nonexclusive inhibitors. *Eur J Biochem* 115:207–216.
48. Geran RI, Greenberg NH, Macdonald MM, Schumacher AM, Abbott BJ (1972) Protocols for screening chemical agents and natural products against animal tumours and other biological systems. *Cancer Chemother Rep* 3:1–104.
49. Generalova AN, et al. (2015) Submicron polyacrolein particles in situ embedded with upconversion nanoparticles for bioassay. *Nanoscale* 7:1709–1717.